BNL-73770-2005-JA

ITO CALCULUS OF THE COMPETITION FOR VAPOR: A NEW STOCHASTIC MODEL OF WATER DROPLET EVOLUTION IN TURBULENT CLOUDS

Robert McGraw and Yangang Liu
Environmental Sciences Department
Atmospheric Sciences Division
Brookhaven National Laboratory
Upton, NY 11973

March 2005

Submitted to
Physical Review E

ABSTRACT

A stochastic model is introduced to represent turbulence-induced fluctuations in water vapor saturation within an atmospheric cloud. These fluctuations, together with the rate law for diffusion-controlled droplet growth, are used to derive fluctuations in growth rate and cloud droplet size. Through analogy with the theory of Brownian motion in an external field of force, we obtain time-dependent current and Fokker-Planck equations for evolution of the cloud droplet size distribution. Under stationary cloud conditions, simple analytic distributions of the Weibull or modified gamma type result, depending on how vapor depletion effects are represented in the model. In the simplest case that all drops within the modeled cloud parcel are subject to uniform depletion the Weibull distribution results. Ito calculus and scaling are used to analyze the stochastic evaporation/growth equations, and results from Monte-Carlo simulations of evolving cloud droplet populations are presented. The new stochastic model provides microphysical foundation for two key cloud parameters, the turbulent diffusion coefficient for fluctuations in droplet size and the effective evaporation rate, employed in the recently developed kinetic potential theory of drizzle formation [1,2].

Research by BNL investigators was performed under the auspices of the U.S. Department of Energy under Contract No. DE-AC02-98CH10886.

1. **Introduction**

Uncertainties associated with the physical processes governing clouds and precipitation limit both regional weather forecast accuracy and the ability to predict future global climate using computer models [3]. A large component of this uncertainty derives from complications associated with the coupling between cloud turbulence and microphysical processes over a wide range of spatial/temporal scales and droplet size [4]. Much effort is currently aimed at reducing uncertainty through the development of more robust parameterizations for clouds and precipitation that are microphysically based yet computationally simple enough so as to be suitable for use in regional to global scale models (e.g., Ref. 5). Especially crucial to understanding many cloud-related phenomena such as precipitation, optical properties, and assessment of the climate impact of anthropogenic aerosols through indirect effects related to the tendency for aerosols to alter cloud properties, is knowledge of the cloud droplet size distribution. Recent progress in parameterizations for clouds and precipitation in atmospheric models [6,7], indirect aerosol effects [8], and rain initiation theory [1,2] reinforces the need for better understanding of the spectral shape of the droplet size distribution.

In the following sections we introduce a new stochastic model for representing the effect of turbulence on the condensation and evaporation processes that govern droplet growth in a non-precipitating cloud. Theoretical results are obtained for fluctuations in individual droplet size and for the size distribution function for an ensemble of droplets in a stationary cloud. The results are in excellent agreement with both measured cloud drop size distributions [6,9] and with the most probable distributions derived from the application of systems theory to clouds [10,11].

Although significant progress in our understanding of the cloud droplet size distribution has been made over the last few decades, the details of the processes involved are still poorly understood and highly controversial. Furthermore, few studies/models have provided analytical forms for the droplet size distribution that agree well with observations. A long-standing problem in cloud physics is that observed droplet size distributions are generally much broader than those predicted by the classical uniform model [12]. To explain this so-called spectral broadening has been a major focus of cloud physics over the last few decades, and a number of models have been proposed. Early attempts in 1960's employed a condensation theory that considered the growth of droplet populations as a stochastic process and related spectral broadening to various fluctuations associated with turbulence [13,14]. Efforts along similar lines have continued to date. For example, Cooper [15] derived equations for estimating the spectral width of droplet size distributions from fluctuations in vertical velocity and integral radius, and their correlation, by applying small perturbation analysis to the Lagrangian integral of the quasi-steady supersaturation averaged over an ensemble of droplets that encounter different growth trajectories through turbulent clouds. Srivastava [16] argued that the supersaturation that controls each individual droplet (microscopic supersaturation) differs from the commonly used macroscopic supersaturation. There it was shown that even without turbulence a Poisson spatial distribution of droplets could cause droplet-droplet variations in the microscopic supersaturation, which in turn leads to some spectral broadening. Shaw et al. [17] relate spectral broadening to supersaturation fluctuations caused by turbulence-induced preferential concentration of droplets.

Another school has focused its effort on the processes of turbulent entrainment and mixing as causes of spectral broadening [18-21].

Previous models of stochastic condensation have usually been of the mean field type. In these models a collection of droplets, estimated on the basis of Kolmogorov scaling to be several meters in extent [4], is uniformly subject to a low-frequency fluctuating saturation tied to the vertical updraft velocity. However, it has been shown that this uniformity places a severe restriction on the degree to which turbulent fluctuations can lead to broadening of the size distribution [22]. After pointing out that the early stochastic condensation models generally yield droplet size distributions of the Gaussian type while observations tend to follow positively skewed distributions, Khvorostyanov and Curry [23,24] derived a more general mean-field equation that yields gamma droplet size distributions under certain assumptions in the low-frequency regime. Nevertheless, it is clear that the low-frequency limit is often not satisfied in clouds, where significant turbulence fluctuations can occur on smaller spatial scales [4].

An alternative (non-mean field) approach was described by Kulmala et al. [25]. This approach, also used the present study, captures fluctuations on the smaller spatial scales by sampling the condensation/evaporation trajectories of individual droplets each allowed to experience a different fluctuation history – thus providing a statistical sampling of the droplet distribution. The droplet growth trajectories are assumed to be driven by turbulence fluctuations in vapor saturation. Effects from vapor depletion (e.g. on slowing of droplet growth and approach to a stationary size spectrum), were not included in the simulations of Ref. 15; but such effects are a major focus of the present study.

The new stochastic model is introduced in Sec. 2. Here we reformulate the stochastic condensation theory by deriving a corresponding Langevin equation for fluctuating droplet size. The analytic methods are analogous to those used in the theory of Brownian motion in an external field of force; with turbulence responsible for diffusion along the coordinate of droplet size, and the "force" derived as a consequence of vapor depletion. The methods of Ito calculus, employed in Sec. 3, formally bridge the transition from fluctuations in individual droplet size to the ensemble via the development of a time-dependent Fokker-Planck equation for evolution of the droplet size distribution. Under stationary cloud conditions, solution of the Fokker-Planck equation yields analytical droplet size distributions of the Weibull or modified gamma type - depending on how vapor depletion is represented in the model. Ito calculus and scaling are used to analyze the stochastic growth equations in Sec. 4. Monte-Carlo simulations for evolving droplet populations coupled through the vapor, so as to include depletion effects, are carried out in Sec. 5 and shown to compare favorably with the theoretical predictions.

Section 5 includes a reexamination of the theoretical foundation for the recent kinetic potential (KP) model of rain initiation [1,2] in light of these new results. The KP model accounts for turbulent condensation and evaporation, but previously represented these processes in a much more *ad-hoc* fashion than is now possible with the new results. For example, condensation was represented by a single turbulence parameter together with a corresponding "effective evaporation rate" defined so as to yield a prescribed droplet size distribution through detailed balance [1,2]. The present analysis yields deeper physical insight into the turbulent

condensation/evaporation processes basic to the KP model: The turbulent condensation parameter, proportional to the diffusion rate for droplet fluctuations in size space, is now given in terms of the variance and correlation time of fluctuations in vapor saturation arising from turbulence (Sec. 2), both of which are capable of estimation from measurements (Sec. 5). The effective evaporation rate is shown to be a quantifiable consequence of vapor depletion (Appendix B), and the droplet size distribution, previously prescribed, is now derived from the stochastic model itself.

Stochastic droplet growth model

2.1 Fluctuations in local supersaturation

As cloud droplets are significantly larger than the mean free path of the surrounding air, droplet growth occurs in the continuum, or diffusion limited, regime [22]:

$$\frac{d}{dt}r^2 = k(T)(S-1) \qquad (2.1)$$

Here r is droplet radius, $k(T)$ is a temperature and pressure dependent rate coefficient (to simplify notation we suppress the weaker pressure dependence) and S is the saturation ratio, defined as the ratio of the vapor pressure of the interstitial cloud air to the equilibrium vapor pressure of the drop. For example, at $T = 10^{\circ}C$ and pressure of 800 mb, $k(10^{\circ}C) = 167.8$ ($\mu m^2 s^{-1}$), as determined from Eq. 13.28 and the parameters given in Table 13.1 of Pruppacher and Klett [22]. This calculation takes into account the thermophysical properties of water and includes coupled heat and mass transfer during growth/evaporation of the drop [22]. *k(T)* is shown as a function of temperature in Fig. 1.

We consider further that, due to turbulence, S fluctuates over time and that these fluctuations give rise to corresponding fluctuations, via Eq. 2.1, in the rates of droplet

growth. Allowing for the possibility that the mean saturation ratio, $\langle S \rangle$, differs from unity, Eq. 2.1 can be trivially rewritten to identify the uniform and fluctuating contributions to droplet growth:

$$\frac{d}{dt} r^2 = k(T)\left(\langle S \rangle - 1\right) + k(T)\left(S(t) - \langle S \rangle\right). \tag{2.2}$$

Angular brackets denote averaging over the ensemble of droplets present in the parcel of cloud under study. The first and second terms on the right hand side give the uniform and fluctuation contributions, respectively, to droplet growth. The instantaneous saturation ratio, $S(t)$, is assumed to vary from drop to drop within the same parcel, for droplets that are sufficiently far apart, thus enabling the parcel droplets to collectively sample the fluctuations in *S*. Thus in this model the vapor saturation arises from two contributions: a random component and a uniform shift, $\langle S \rangle - 1$. The latter may also include a time dependence arising, for example, during adiabatic cooling of a parcel of cloud air. More significant to the present study is the finding, in Sec. 3, that vapor depletion also manifests itself as a shift in $\langle S \rangle$, to values below unity, that persist even under stationary cloud conditions. To present the simplest case for analysis first, we will initially assume that $\langle S \rangle$ is uniform throughout the cloud parcel. In Sec. 6 this assumption is relaxed to allow for the possibility that vapor depletion and $\langle S \rangle$ are correlated locally with droplet size. There we also examine the case that the evaporation rate is correlated with droplet size through the Kelvin effect.

Ideally one would like to evaluate the fluctuations in *S* from turbulence probability distribution function (pdf) data, as was done in a study of the homogeneous nucleation of water vapor in a free turbulent jet [16]. Unfortunately, such detailed information on the pdf does not appear to be available for clouds and additional model

assumptions are required to make further progress. Here we will assume: (i) that the fluctuations in S can be characterized by a finite second moment, or variance σ_S^2,

$$\left\langle \left(S(t) - \langle S \rangle \right)^2 \right\rangle = \sigma_S^2; \tag{2.3a}$$

(ii) the persistence, or memory, of these fluctuations decays exponentially over a correlation timescale γ^{-1}; (iii) the fluctuations are stationary in the sense that their statistical properties are independent of time. Under (ii) and (iii), the auto-correlation function takes the form:

$$\begin{aligned} &\left\langle \left(S(t) - \langle S \rangle \right) \left(S(t+\Delta) - \langle S \rangle \right) \right\rangle = \langle S(t) S(t+\Delta) \rangle - \langle S \rangle^2 \\ &\langle S(0) S(\Delta) \rangle - \langle S \rangle^2 = \sigma_S^2 \exp(-\gamma \Delta) \end{aligned} \tag{2.3b}$$

for time intervals, Δ, short compared to the time scale, τ, of significant change in the average properties of the cloud (Sec. 4). Supersaturations in the atmosphere are thought to only rarely exceed a few percent and the allowed range for σ_S should be chosen so as to give typical fluctuations less than that amount. Kulmala et al. [25] employed the same auto-correlation function as Eq. 2.3b and further assumed a gaussian for the distribution of $S(t)$. It is significant that the analysis of Secs. 2.2 and 2.3 requires only the first and second moments of $S(t)$, appearing in Eqs. 2.3, and not its full distribution. This has two advantages: First, the analysis applies even in the face of large (non-gaussian) fluctuations in $S(t)$ from intermittency – a well known property of cloud turbulence [4]. Second, an analytic expression is obtained directly for the rate of diffusion along the droplet size coordinate (Eq. 2.14 below), which is an important parameter in the KP rain initiation theory (Appendix B).

It is equally important to consider the reverse process – whereby the droplet population affects saturation levels in the cloud. Thus the parameters σ_S^2 and γ may be

influenced by the condensation process itself as, for example, excursions to positive (negative) values of *S*-1 tend to be offset by condensation (evaporation) resulting in a damping of the amplitude of the fluctuations in *S*. Also, fluctuations in saturation are likely correlated with fluctuations in local droplet number concentrations and liquid water content [16], the average values of which we will treat as fixed inputs to the model, and droplet size. Initially we will assume fixed values for $\sigma_S^{\,2}$ and γ, relaxing this assumption in Sec. 6 to allow for possible correlations with droplet size.

2.2 Diffusion of droplet size

Introducing the velocity along the growth coordinate, $z \equiv r^2$:

$$v(t) \equiv \frac{dz}{dt} = \frac{dr^2}{dt}, \tag{2.4}$$

Eqs. 2.2 and 2.3 combine to give:

$$\langle v(t)v(t+\Delta)\rangle = \langle v(0)v(\Delta)\rangle = \bar{v}^2 + \langle \delta v(0)\delta v(\Delta)\rangle = \bar{v}^2 + k^2(T)\sigma_S^{\,2}\exp(-\gamma\Delta) \tag{2.5}$$

where $v = \bar{v} + \delta v$ with

$$\bar{v} = k(T)\big(\langle S\rangle - 1\big) \tag{2.6a}$$

and

$$\delta v(t) = k(T)\big(S(t) - \langle S\rangle\big). \tag{2.6b}$$

The first equality of Eq. 2.5 results from the time-stationary assumption (iii) and the second from the vanishing of cross terms.

Positive (negative) values of $v(t)$ signify that the droplet is undergoing growth (evaporation) at time *t*, causing fluctuations in saturation to result in fluctuations in droplet size. A quantitative description of this effect can be obtained as follows. Let:

$$\Delta z(t) \equiv z(t) - z(0) = \int_0^t v(t')\,dt'$$

where $v(t)$ is the growth velocity of a particular drop in the parcel whose initial size is $z(0)$. Thus,

$$\Delta z^2(t) = \int_0^t dt' \int_0^t \langle v(t')v(t'')\rangle dt''$$

and

$$\begin{aligned}\frac{d}{dt}\Delta z^2(t) &= 2\langle v(t)[z(t)-z(0)]\rangle = 2\langle v(0)[z(0)-z(-t)]\rangle \\ &= 2\int_{-t}^{0}\langle v(0)v(-t')\rangle dt' = 2\int_0^t \langle v(0)v(t')\rangle dt' = 2\int_0^t \langle \delta v(0)\delta v(t')\rangle dt' + 2\bar{v}^2 t\end{aligned} \tag{2.7}$$

where the last equalities result from shifting the time origin, as allowed by the assumption of stationarity, and commuting the order of the product in angular brackets. Finally, substitution for the correlation function from Eq. 2.5 into the last integral gives:

$$\frac{d}{dt}\Delta z^2(t) = 2k^2(T)\sigma_S{}^2\int_0^t \exp(-\gamma t')dt' + 2\bar{v}^2 t = 2\frac{k^2(T)\sigma_S{}^2}{\gamma}[1-\exp(-\gamma t)] + 2\bar{v}^2 t$$

or, in integrated form,

$$\Delta z^2(t) = 2\frac{k^2(T)\sigma_S{}^2}{\gamma}\left\{t - \frac{1}{\gamma} + \frac{1}{\gamma}\exp(-\gamma t)\right\} + \bar{v}^2 t^2. \tag{2.8}$$

For times long compared to $1/\gamma$, the exponential factor is less than unity and Δz^2 is dominated by the contributions from drift motion (term proportional to t^2) and diffusion (term proportional to t).

For diffusion along a single coordinate (here z) the diffusive contribution to the mean square displacement goes as $2D_Z t$, where D_Z is the diffusion coefficient, and Eq. 2.5 yields the diffusion coefficient for fluctuations in droplet size:

$$D_Z = \int_0^t \langle \delta v(0)\delta v(t')\rangle dt' = k^2(T)\int_0^t \langle (S(0)-\langle S\rangle)(S(t')-\langle S\rangle)\rangle dt' = \frac{k^2(T)\sigma_S{}^2}{\gamma}. \tag{2.9}$$

The first equality is the most general and has the form of a Green-Kubo relation between a transport coefficient (here D_Z) and the time integral of an auto-correlation function [27]. This follows already from Eq. 2.7. The last expression for D_Z, which is the one most frequently employed in the calculations below, follows Eq. 2.8 and is specific to the saturation auto-correlation function model of Eq. 2.3.

2.3 Stochastic differential equation for droplet growth

Further progress is achieved through the development of stochastic differential equations for evolution of the droplet growth rate and droplet size. We begin with the conjecture of a Langevin-like stochastic differential equation for the fluctuating part of the growth rate and show that this is compatible with the fluctuation model of Secs. 2.1 and 2.2:

$$\frac{d(\delta v)}{dt} = -\gamma(\delta v) + A(t) \tag{2.10}$$

where $\delta v = v - \overline{v}$ and $A(t)$ is the underlying "random force", representing the effect of turbulence on fluctuations in v and droplet size. From the standpoint of hydrodynamics, Eq. 2.10 describes a single-relaxation-time Debye model of hydrodynamic mode decay [28]. The Langevin description provides an alternative picture for the evolution of droplet growth velocity that is fully compatible with Eqs. 2.3 and 2.5. To show this equivalence, note that the formal solution to Eq. 2.10 is:

$$\delta v(t) = \delta v(0)\exp(-\gamma t) + \int_0^t \exp\left[-\gamma(t-t')\right]A(t')dt' . \tag{2.11}$$

Multiplying on the left by $\delta v(0)$ and averaging using the property that the random force is uncorrelated with the initial velocity displacement ($\langle \delta v(0)A(t') \rangle = 0$, one obtains:

$$\langle \delta v(0)\delta v(t) \rangle = \langle \delta v(0)\delta v(0) \rangle \exp(-\gamma t) = k^2(T)\sigma_S{}^2 \exp(-\gamma t) \tag{2.12}$$

in agreement with Eq. 2.5.

Stochastic properties of the fluctuating drop size are also obtainable from Eqs. 2.10 and 2.4. Indeed one can draw a close analogy and think of these equations as representing the velocity and position, respectively, of a particle undergoing Brownian motion in a fluid [29]. Under conditions that the time scales of interest exceed $1/\gamma$, the Brownian particle is overdamped, and a similar Langevin equation can be written that involves the spatial coordinate alone (i.e., one that is not explicitly dependent on the fluctuating velocity component δv) [29]. The result, in notation advantageous to the application of Ito calculus [30], is a similar stochastic differential equation:

$$dz = \bar{v}dt + \sigma_z dX \tag{2.13}$$

whose study is the main focus of the present work. The lead term on the right contains the "drift velocity" $\bar{v}$, which in the Brownian analogy corresponds to the case of a particle undergoing Brownian motion in an external field of force, here independent of the coordinate z.

Exceptionally lucid descriptions of the formal methods required for analysis and numerical simulation of stochastic differential equations of this type are available, perhaps due in part to their widespread use in the pricing of options and other "derivatives" by the financial industry [30]. The quantity dt appearing in Eq. 2.13 is to be regarded as a small physical interval of time - small enough that the change in z is small while the saturation still has time to fluctuate. The lead term on the right hand side gives the deterministic contribution to the growth rate and presents no special difficulty. The fluctuation term with

$$\sigma_Z{}^2 = 2D_Z = 2\frac{k^2(T)\sigma_S}{\gamma} \tag{2.14}$$

can be integrated using the methods of Itô calculus. Following [30], the latter is implemented by setting $dX = \phi\sqrt{dt}$ where ϕ is a dimensionless random variable drawn from a standardized normal distribution with zero mean and unit variance:

$$\frac{1}{\sqrt{2\pi}}\exp(-\phi^2/2).$$

Defining the expectation value of a quantity $F(\phi)$ as:

$$\langle F(\phi)\rangle = \frac{1}{\sqrt{2\pi}}\int_{-\infty}^{\infty} F(\phi)\exp(-\phi^2/2)d\phi$$

it is seen that

$$\begin{aligned}\langle dX\rangle &= 0\\ \langle dX^2\rangle &= dt\end{aligned} \tag{2.15}$$

Note that $\sigma_Z{}^2$ is a measure of the volatility of fluctuations in z and is not the variance of this coordinate, which in general is time dependent (cf. Eq. 2.8). Squaring Eq. 2.13 and averaging gives:

$$\langle dz^2\rangle = \bar{v}^2(dt)^2 + \sigma_Z{}^2\langle dX^2\rangle = \bar{v}^2(dt)^2 + 2\frac{k^2(T)\sigma_S{}^2}{\gamma}(dt) \tag{2.16}$$

in agreement with Eq. 2.8 for the overdamped regime characterized by time scales for significant droplet growth that exceed the saturation auto-correlation time, $1/\gamma$. This assumption of time scale separation is supported *a posteriori* from results obtained in Sec. 5.

3. Fokker-Planck equation for the distribution of droplet size

Thus far we have considered excursions in droplet size for a single drop and turn next to the more relevant question of calculating the distribution of droplet size. For an ensemble of droplets Eq. 2.13 is in one-to-one correspondence with a unique Fokker-

Planck equation for the distribution. Following standard rules for handling stochastic differential equations summarized in the Appendix A, this is:

$$\frac{\partial f}{\partial t} = D_Z \frac{\partial^2 f}{\partial z^2} - \bar{v}\frac{\partial f}{\partial z} = \frac{k^2(T)\sigma_S^{\,2}}{\gamma}\frac{\partial^2 f}{\partial z^2} - \bar{v}\frac{\partial f}{\partial z} \tag{3.1}$$

where $f(z,t)$ is the continuous distribution function giving the number of droplets per unit volume within the size range z to $z+dz$ at time t. The first and second terms on the right hand side account for diffusion and drift along the z coordinate, respectively. In general $\bar{v}$ will vary with changes in liquid water content during approach to the stationary droplet distribution state, thus precluding a simple analytic solution for the time-dependent case. In this section we focus on the stationary limit of Eq. 3.1 for which analytic results are easily obtained. Time-dependent behavior is examined as part of the numerical simulations presented in Sec. 5.

The Fokker-Planck equation can also be cast in terms of the droplet current, $J(z)$, defined as the net flux of droplets passing through z in the direction of increasing size. The result is the equivalent continuity equation:

$$\frac{\partial f}{\partial t} = -\frac{\partial J}{\partial z} \tag{3.2a}$$

with

$$J(z) = -D_Z \frac{\partial f(z)}{\partial z} + \bar{v} f(z)\,. \tag{3.2b}$$

In the absence of droplet sources and sinks, $J(z) = 0$ for a stationary droplet distribution. Integration of Eq. 3.2b for this case yields:

$$f_\infty(z) = N_D \frac{|\bar{v}_\infty|}{D_Z} \exp(\bar{v}_\infty z / D_Z) \tag{3.3}$$

for $z \geq 0$ and normalization to the cloud droplet number concentration N_D. The new subscript denotes the stationary distribution. Normalization of requires that $\bar{v}_\infty = -|\bar{v}_\infty|$ be negative - implying the tendency towards evaporation to smaller droplet sizes. Under stationary conditions, just enough evaporation takes place to balance the tendency toward increasing droplet size through diffusion, which of course is limited to the positive growth coordinate *z*. This balance of currents is illustrated in the top panel of Fig. 2.

The liquid water fraction (cm^3 cloud liquid water/ cm^3 air) is obtained as the 3/2 moment of $f(z)$:

$$L = \frac{4\pi}{3}\int_0^\infty z^{3/2} f(z) dz \,. \tag{3.4a}$$

and

$$L_\infty = \pi^{3/2} N_D \left(\frac{D_Z}{|\bar{v}_\infty|} \right)^{3/2} \tag{3.4b}$$

following substitution for the stationary distribution from Eq. 3.3. This last result provides a determination of $\bar{v}_\infty$:

$$\bar{v}_\infty = -\pi \left(\frac{N_D}{L} \right)^{2/3} D_Z = -\pi \left(\frac{N_D}{L} \right)^{2/3} \frac{k^2(T)\sigma_S^{\,2}}{\gamma} \tag{3.5}$$

Equation 3.5 describes the velocity in droplet size space generated by the "force" that results from vapor depletion in a stationary cloud. Reflective of vapor depletion, the theory predicts a uniform shift in the average saturation to values below unity. Under stationary conditions (c.f. Eq. 2.6a):

$$\bar{v}_\infty = k(T)\left(\langle S \rangle_\infty - 1 \right)$$

or

$$\langle S \rangle_\infty = 1 - \pi \left(\frac{N_D}{L} \right)^{2/3} \frac{k(T)\sigma_S^{\,2}}{\gamma}. \qquad (3.6)$$

This result provides a quantitative determination of the vapor depletion effect that results from droplet competition for water vapor. In the absence of fluctuations ($\sigma_S^{\,2} = 0$), $\bar{v}_\infty = 0$, and the water vapor is in equilibrium with the droplets at $S = 1$.

Transforming Eq. 3.3 to the radial coordinate and substituting for $|\bar{v}_\infty| / D_Z$ from Eq. 3.5 gives the corresponding radial distribution function:

$$n_\infty(r) = 2\pi N_D \left(\frac{N_D}{L} \right)^{2/3} r \exp\left[-\pi \left(\frac{N_D}{L} \right)^{2/3} r^2 \right] \qquad (3.7)$$

normalized to the droplet number concentration N_D. This is a Weibull distribution that, remarkably, depends solely on the cloud parameters N_D and L. Figure 2 shows the distributions from Eqs. 3.3 (top panel) and 3.7 (bottom panel) for a typical maritime cloud condition $N_D = 100 cm^{-3}$, $L = 5.0 \times 10^{-7}$. At this loading the mean cloud droplet radius obtained from Eq. 3.7 is $8.55 \mu m$, which is typical for a cloud. Both distributions are normalized on the micron scale to the droplet number concentration N_D.

4. Scaling

For economy of computation and parameterization it is convenient to introduce scaled variables and scaled distributions using the parameters defined in Table 1:

Scaled variables	Scaling parameters
$\tilde{z} = z / z_0$ $\tilde{t} = t / \tau$ $\tilde{v} = v / v_0$ (drift velocity) $\tilde{r} = r / r_0$ (radius) $d\tilde{X} = dX / \sqrt{\tau}$	$z_0 = (3/4\pi)^{2/3} (L/N_D)^{2/3}$ $\tau = z_0^2 / (2D_Z) = (1/2)(3/4\pi)^{4/3} (L/N_D)^{4/3} \gamma / [k^2(T)\sigma_S{}^2]$ $v_0 = z_0 / \tau = 2(4\pi/3)^{2/3} k^2(T)\sigma_S{}^2 (N_D/L)^{2/3} / \gamma$ $r_0 = +\sqrt{z_0} = (3/4\pi)^{1/3} (L/N_D)^{1/3}$

Table 1. Scaled variables and scaling parameters defined in terms of cloud microphysical properties.

Simulations carried out in terms of scaled variables for a single reduced distribution function are immediately representative of an entire family of cloud droplet distributions having different values for the microphysical properties appearing in the right hand sides of the equations included in the second column of Table 1.

From the last entry of the first column:

$$\left\langle d\tilde{X}^2 \right\rangle = \left\langle dX^2 \right\rangle / \tau = dt / \tau = d\tilde{t} \tag{4.1}$$

and Eq. 2.13 becomes:

$$d\tilde{z} = \tilde{\bar{v}}\, d\tilde{t} + d\tilde{X} \tag{4.2}$$

with $\left\langle d\tilde{X} \right\rangle = 0$ and $\left\langle d\tilde{X}^2 \right\rangle = d\tilde{t}$. In scaled coordinates, the Fokker-Planck equation (Eq. 3. 1) takes the reduced form:

$$\frac{\partial \tilde{f}}{\partial \tilde{t}} = \frac{1}{2} \frac{\partial^2 \tilde{f}}{\partial \tilde{z}^2} - \tilde{\bar{v}} \frac{\partial \tilde{f}}{\partial \tilde{z}} \tag{4.3}$$

where $\tilde{f}(\tilde{z}) = f(z)(dz/d\tilde{z}) = z_0 f(z)$ is the transformed distribution function and $d\tilde{f} = z_0 df$. Under stationary cloud conditions Eq. 4.3 gives the normalized solution

$$\tilde{f}_\infty(\tilde{z}) = 2\left|\tilde{\bar{v}}_\infty\right| \exp(2\tilde{\bar{v}}_\infty \tilde{z}) \tag{4.4}$$

where $\left|\tilde{\bar{v}}_\infty\right|$ is the absolute value of the reduced stationary drift velocity. The latter quantity is not arbitrary as we require that the integrated distribution yield the specified liquid water content, L/N_D for the normalized distribution. This requires, in particular:

$$\frac{L}{N_D} = \frac{4\pi}{3} z_0^{3/2} \int_0^\infty \tilde{z}^{3/2} \tilde{f}_\infty(\tilde{z}) d\tilde{z} = \frac{4\pi}{3} \Gamma(5/2) \left(\frac{z_0}{2\left|\tilde{\bar{v}}\right|_\infty} \right)^{3/2} = \pi^{3/2} \left(\frac{3}{4\pi} \right) \left(\frac{1}{2\left|\tilde{\bar{v}}\right|_\infty} \right)^{3/2} \frac{L}{N_D}.$$

The second equality follows substitution from Eq. 3.4 for the stationary distribution and the last equality gives

$$\tilde{\bar{v}}_\infty = -\left|\tilde{\bar{v}}_\infty\right| = -\frac{\pi}{2} \left(\frac{3}{4\pi} \right)^{2/3} = -0.604497... \equiv -d_0 \tag{4.5}$$

defining the numerical constant d_0. Thus the final form for the scaled distribution is:

$$\tilde{f}_\infty(\tilde{z}) = 2 d_0 \exp\left[-2 d_0 \tilde{z}\right], \tag{4.6}$$

which upon transformation to the reduced droplet radial coordinate becomes:

$$\tilde{n}_\infty(\tilde{r}) = 4 d_0 \tilde{r} \exp\left[-2 d_0 \tilde{r}^2\right]. \tag{4.7}$$

where $\tilde{r} = +\sqrt{\tilde{z}}$ is the reduced radius. Transforming and restoring units using $r = +\sqrt{z_0}\, \tilde{r}$ gives:

$$n_\infty(r) = 2\pi \left(\frac{N_D}{L} \right)^{2/3} r \exp\left[-\pi \left(\frac{N_D}{L} \right)^{2/3} r^2 \right] \tag{4.8}$$

in agreement with Eq. 3.7 except for the normalization here to unity.

5. Calculations

In order that a Langevin model provide an unambiguous recipe for numerical simulation, it is first necessary that a consistent set of rules for integration of the stochastic differential equation be chosen [31]. Here we follow the methods of the Ito calculus. The integrated form of Eq. 2.13 gives the size of the drop at time *t*:

$$z(t) - z(t_0) = \int_{t_0}^{t} \bar{v}\, dt + \int_{t_0}^{t} \sigma_Z dX\,. \tag{5.1}$$

The first integral is in standard calculus form and presents no difficulty. The second integral, over *dX*, is an Itô stochastic integral, which can be evaluated numerically as the partitioning of the time interval $t - t_0$ into *m* equal smaller steps $t_0 < t_1 \cdots < t_m = t$ in the limit of large *m* [30]:

$$\int_{t_0}^{t} \sigma_Z dX \approx \sigma_Z \sum_{i=0}^{m-1} \big(X(t_{i+1}) - X(t_i)\big). \tag{5.2}$$

Each increment in parenthesis is drawn from the random distribution: $dX = \phi\sqrt{h}$, where $h = (t - t_0)/m$, corresponding to the physical time increment, *dt*, of Eq. 2.15, is the step duration and ϕ is a dimensionless random variable drawn from a standardized normal distribution with zero mean and unit variance as described in Sec. 2.

Monte-Carlo simulations were carried out for an *N*-drop ensemble of growth/ evaporation trajectories based on Eq. 5.2. For this purpose it is convenient to employ vector notation with each element of the vector referring to one of the drops. At the beginning of each time step, *N* random values,$\{\phi_i\}$, are sampled from the normal distribution with zero mean and unit variance. Each of these values is then multiplied by $\sqrt{h}$ to give the elements of the *N*-component vector $\mathbf{dX}$:

$$\mathbf{dX} = \sqrt{h}\begin{pmatrix} \phi_1 \\ \vdots \\ \phi_N \end{pmatrix}. \tag{5.3}$$

Addition of $\mathbf{dX}$ to the vector of droplet coordinates from the previous time step:

$$\mathbf{z}(t_{k-1}) = \begin{pmatrix} z_1(t_{k-1}) \\ \vdots \\ z_N(t_{k-1}) \end{pmatrix} \tag{5.4}$$

gives the partially updated coordinates,

$$\mathbf{z}^{\mathbf{I}}(t_k) = \mathbf{z}(t_{k-1}) + \sigma_Z \mathbf{dX},$$

which already include the contribution from the random component of turbulent condensation growth. The superscript denotes intermediate coordinates at time step t_k. Finally, a shift in coordinates, $h\bar{\mathbf{v}}(t_k)$, from the depletion term in Eq. 4.2 is added to $\mathbf{z}^{\mathbf{I}}(t_k)$ to get the final updated coordinates, $\mathbf{z}(t_k)$.

The N elements of $\bar{\mathbf{v}}$ are identical, each equal to $\bar{v}$, as the present calculations neglect correlation of drift with droplet size, and generally time dependent. As in Eq. 3.5, $\bar{v}$ is determined, from the liquid water fraction, L. Note that L cannot change significantly, unless either the temperature or total water content (liquid plus vapor) within the parcel changes, due to the fact that the vapor saturation is constrained to be close to unity when liquid water is present. For an adiabatically cooling cloud parcel, L will generally increase with time due to additional water vapor condensation in the absence of any liquid removal processes. Simulations for adiabatic parcels will be presented in future work. For the present calculations we will continue to assume stationary values for the variables, T, P, N_D, and L within the cloud parcel under consideration. To compute $\bar{v}$ we begin by defining the model liquid water content at time step t_k as the total volume of the simulated drops:

$$L_M(t_k) = \frac{4\pi}{3}\sum_{i=1}^{N}[z_i(t_k)]^{3/2} \equiv \frac{4\pi}{3}\mu_{3/2}[\mathbf{z}(t_k)], \tag{5.5}$$

where the subscript, M, distinguishes the model liquid water content from the cloud liquid water fraction. The last equality defines the 3/2 moment of z, $\mu_{3/2}$, at time t_k.

Assuming good sampling, L_M will be proportional to L, thus requiring that L_M also be constant, or nearly constant, throughout the simulation.

On average, the intermediate coordinates $\mathbf{z}^{\mathbf{I}}(t_k)$ will have higher model liquid water content than $\mathbf{z}(t_{k-1})$. This is because diffusion along z in the absence of vapor depletion tends to give increasingly higher values of L_M. Including vapor depletion corrects for this failure to conserve total water content in the parcel. We simulate the effect of depletion, after computation of $\mathbf{z}^{\mathbf{I}}(t_k)$, by shifting the value of each component z_i a constant amount δz (equal to $h\bar{v}$) and determine $\bar{v}$ from the shift that restores $L_M(t_k)$ to its initial value, or more generally its prescribed value, $L_M(0)$. (Note that the shift will never be large because the previous value $L_M(t_{k-1})$ has already been so restored.) The required z-shift is obtained from Eq. 5.5 and its derivative with respect to the shift in z. For this purpose we introduce, in addition to $\mu_{3/2}$, the 1/2 moment:

$$\mu_{1/2}[\mathbf{z}(t_k)] = \sum_{i=1}^{N} [z_i(t_k)]^{1/2}, \tag{5.6}$$

and obtain the correction as

$$\delta z(t_k) = -\frac{2}{3}\frac{\{\mu_{3/2}[\mathbf{z}^{\mathbf{I}}(t_k)] - \mu_{3/2}[\mathbf{z}(0)]\}}{\mu_{1/2}[\mathbf{z}^{\mathbf{I}}(t_k)]}. \tag{5.7}$$

Finally, we obtain the depletion velocity from:

$$\bar{v}(t_k) = \frac{\delta z(t_k)}{h} \tag{5.8}$$

and the updated droplet size coordinates

$$\mathbf{z}(t_k) = \mathbf{z}(t_{k-1}) + \sigma_Z \mathbf{dX} + h\bar{\mathbf{v}}(t_k). \tag{5.9}$$

Positive values for the droplet size coordinates, $\{z_i\}$, are insured by applying a reflective boundary condition at the origin.

Figure 3 shows results from simulations carried out for the reduced Langevin equation, Eq. 4.2, using an ensemble of 100 drops. The model time step was set at $h = 0.001\tau$ ($d\tilde{t} = 0.001$) and the simulation carried out to $t = 5\tau$, or $\tilde{t} = 5$. The initial droplet distribution is taken to be monodisperse with $\tilde{z} = 1$. The top panel of Fig. 3 shows the cumulative radial distribution corresponding to the Weibull distribution, Eq. 4.7:

$$c(\tilde{r}) = \int_0^{\tilde{r}} \tilde{n}_\infty(s)ds\,, \tag{5.10}$$

solid curve, and comparison with results from combining the 100-drop Monte-Carlo simulations at four different times in the stationary limit near $\tilde{t} = 4$ (400 points total).

The bottom panel of Fig. 3 shows evolution of the relative dispersion, a measure of the width of the size distribution defined in terms of the radial moments:

$$\begin{aligned} m_1(\tilde{t}) &= \int_0^\infty \tilde{r}\tilde{n}(\tilde{r},\tilde{t})d\tilde{r} \\ m_2(\tilde{t}) &= \int_0^\infty \tilde{r}^2\tilde{n}(\tilde{r},\tilde{t})d\tilde{r} \end{aligned} \tag{5.11}$$

as [8]:

$$\varepsilon(\tilde{t}) = \frac{\sqrt{m_2(\tilde{t}) - m_1{}^2(\tilde{t})}}{m_1(\tilde{t})}. \tag{5.12}$$

Each of the 5000 points in the figure represents the value of the dispersion at time step *k*: $\varepsilon(\tilde{t}_k)$. Initially the dispersion is zero, corresponding to the monodisperse initial distribution. This is followed by broadening of the distribution with time due to the turbulence fluctuations in saturation and condensation growth/evaporation rate. Note that this behavior is just opposite the tendency of condensation growth at a constant (non-

fluctuating) vapor supersaturation to narrow size distributions over time [32]. Broadening of the distribution is effectively complete at $t = \tau$ ($\tilde{t} = 1$), although there continues to be a slower leveling off to values close to the asymptotic value, $\varepsilon_\infty = 0.5227...$, predicted from the moments of the stationary distribution, Eq. 4.7, and indicated in the figure by the horizontal line.

We turn next to estimation of the range of values likely to be encountered for the model parameters σ_S, γ, and τ. In our previous work we studied a condensation parameter, β^{cond}, which is closely related to D_Z (Appendix B) [1,2]. First we estimated $t_{1\%}(s)$, defined as the time required for diffusion along the growth coordinate to change the cloud droplet size 1% from 10 to 10.1 micron radius, which is inversely proportional to D_Z. Specifically,

$$t_{1\%} \equiv \frac{(\Delta z)^2}{2D_Z} \tag{5.13}$$

where $\Delta z = 10.1^2 - 10.0^2 = 2.01 \mu m^2$ and the units of D_Z are $\mu m^4 s^{-1}$. Comparison with the definition of τ (Table 1) shows the proportionality:

$$t_{1\%} = \frac{(\Delta z)^2}{z_0^{\,2}} \tau \tag{5.14}$$

Figure 4 shows the conditions, $\sigma_S^{\,2} / \gamma$ and temperature (° C), for which $t_{1\%}$ assumes values of 0.1, 1.0, and 10.0 seconds (solid curves). (In the present model, the temperature dependence of D_Z and $t_{1\%}$ derives from the temperature dependence of $k(T)$). Also shown are contours of constant τ from Table 1 for $z_0 = 100 \mu m^2$ corresponding to an average cloud droplet radius of $10 \mu m$. Considering the typical lifetime of clouds, which sets a lower limit on the ordinate, and the maximum saturation

ratio likely to be encountered, which sets an upper limit, it is likely that most values of σ_S^2/γ encountered will fall between the curves for $t_{1\%} = 0.1s$ ($\tau \approx 4min$) and $\tau = 60min$ ($t_{1\%} = 1.5s$). For example, at $T = 10°C$, a 1% variance in the saturation ($\sigma_S = 0.01$) and correlation time ($1/\gamma = 7s$) for fluctuations in S yields $t_{1\%} = 0.1s$. These values for σ_S and $1/\gamma$ are in the range of estimated values for these quantities from Kulmala et al. [25] based on aircraft measurements [33]. Furthermore the yielded value, $t_{1\%} = 0.1s$, is within the range of our previous assignment for this quantity and is a parameter value for which a determination of the threshold conditions for drizzle formation has been carried out [2]. Nevertheless, with the new stochastic model, the microphysical basis for this parameter, and for the effective evaporation rate (Appendix B), are each more firmly established. Shorter correlation times and/or fluctuations of smaller amplitude imply longer relaxation times required to reach stationary cloud conditions. The assumption of the overdamped case (used in Eq. 2.13) requires that $1/\gamma << \tau$. This inequality is consistent with the estimated correlation and relaxation times above, providing an *a posteriei* justification and foundation for the overdamped Brownian model used in Sec. 2.

2. Extensions to size-dependent drift and diffusion rates

More sophisticated models for size-correlated evaporation, growth, and fluctuations in local vapor saturation can be constructed and result in Langevin equations having drift and diffusion coefficients dependent on droplet size. In such cases ambiguities in interpretation of the Langevin equation arise leading to the development of distinct, but internally consistent methods of solution under the headings 'Ito calculus' and 'Stratonovich calculus' [31]. Nevertheless, there is no ambiguity in the integrated results and we have tested both methods and found the droplet distributions obtained

below to be independent of which set of rules (Ito or Stratonovich) is employed. As in the previous sections we continue to follow the methods of Ito calculus (Appendix A). To illustrate we examine two cases: (1) the average saturation ratio is constrained to unity and drift to smaller size occurs due to elevation in droplet vapor pressure and evaporation rate from the Kelvin effect; (2) the inverse problem whereby the droplet size distribution is measured, or specified a priori to have a certain form, for example an exponentially decaying distribution in droplet volume, and we seek to determine size-dependent Langevin coefficients for diffusion and drift.

3. Enhanced evaporation from the Kelvin effect

The elevated saturation ratio in equilibrium with a small solute-free droplet is given by the Kelvin relation [22]:

$$S_{eq}(r) = \exp\left(\frac{2\gamma_\infty}{\rho_l kTr}\right) \approx 1 + \frac{2\gamma_\infty}{\rho_l kTr} = 1 + \frac{2\gamma_\infty}{\rho_l kT} z^{-1/2} \qquad (6.1)$$

where γ_∞ is the surface tension of a flat liquid-vapor interface and ρ_l is the number of molecules per unit volume in the bulk liquid phase. Although the elevation in vapor pressure for cloud droplets is small, compared for example to the root-mean-square fluctuations in vapor pressure expected from turbulent diffusion, its persistent sign and action over the cloud lifetime require that it be taken into account. The linearized approximation of Eq. 6.1 is excellent even for *r* values down to the 0.1 micron range characteristic of the smallest droplets in a cloud. To separate the Kelvin effect for purpose of illustration, we set the average background saturation ratio to unity. In this case the depletion contribution to drift from Eq. 2.6a vanishes, but Eq. 6.1 gives a new, *z*-dependent, mechanism for drift to smaller droplet size:

$$v(z) = \frac{dz}{dt} = k(T)[1 - S_{eq}(r)] = -k(T)\frac{2\gamma_\infty}{\rho_l kT} z^{-1/2} \equiv -v_1 z^{-1/2}. \qquad (6.2)$$

The last equality defines $v_1 > 0$ as the magnitude of the drift velocity for z equal to unity (here 1 micron^2).

Treating the fluctuating contribution to droplet growth as in Secs. 2 and 3, and using Eq. 6.2 for drift, yields size-dependent Langevin and Fokker-Planck equation coefficients in accord with Eqs. A1-A4 (Appendix A):

$$\begin{aligned} A(z) &= \sigma_Z \\ B(z) &= -v_1 z^{-1/2} \\ D^{(2)}(z) &= \frac{A^2(z)}{2} = \frac{\sigma_Z^2}{2} = D_Z \\ D^{(1)}(z) &= B(z) = -v_1 z^{-1/2} \end{aligned} \qquad (6.3)$$

The Fokker-Planck equation constructed from $D^{(1)}$ and $D^{(2)}$ is (Eq. A2):

$$\frac{\partial f}{\partial t} = D_Z \frac{\partial^2 f}{\partial z^2} + \frac{\partial}{\partial z}(v_1 z^{-1/2} f).$$

The stationary solution, obtained by equating both sides to zero, is a gamma distribution in drop radius:

$$n_\infty(r) = N_D \left(\frac{2v_1}{D_Z}\right)^2 r \exp\left(-\frac{2v_1}{D_Z} r\right), \qquad (6.4)$$

normalized here to the droplet number concentration, N_D. This distribution has relative dispersion $\varepsilon_\infty = 1/\sqrt{2}$ and is thus somewhat broader than the Weibull distribution obtained previously. The average droplet water content from Eq. 6.4 is:

$$\frac{L}{N_D} = \frac{4\pi}{3}\int_0^\infty r^3 n_\infty(r) dr = \frac{4}{\pi}\left(\frac{D_Z}{v_1}\right)^3, \qquad (6.5)$$

which relation can be used to recast Eq. 6.4 in terms of the measurable cloud parameters N_D and L.

For water at 10°C, substitution into Eq. 6.2 gives $v_1 \approx 0.19 \mu m^3 s^{-1}$ and the only remaining parameters in Eq. 6.4 are N_D and D_Z. The range of likely values for D_Z can be estimated as in the previous section. Specifically, from our estimated range for $t_{1\%}$

$$0.1s \le t_{1\%} \le 1.5s,$$

we obtain from Eq. 5.13 the corresponding range:

$$20.2 \ge D_Z \ge 1.35 \tag{6.6}$$

for D_Z. Expressing volume in cgs units and combining this result with Eq. 6.5 with the determination of v_1 we obtain:

$$1.5 \times 10^{-6} \ge \frac{L}{N_D}(cm^3) \ge 4.5 \times 10^{-10} \tag{6.7}$$

for the average droplet volume. Although this is a wide range, it remains noteworthy that it includes the conditions spanned by typical clouds (e.g. L values of order 10^{-5} to 10^{-6} and N_D values in the range 50-1000 cm^{-3}). This would not be the case but for the similar enhancements of evaporation rate found from the Kelvin and vapor depletion effects – this despite the very different physics behind these two processes.

The combination of turbulent diffusion and the Kelvin effect results in a simple analytic form for the droplet spectrum (Eq. 6.4). However, for values of D_Z lying towards the upper end of the range set by Eq. 6.6, the average size of the droplets obtained from Eq. 6.7 exceeds the observed range of cloud droplet size. This is because the Kelvin effect, alone, is insufficient to maintain the small droplet sizes of typical clouds under higher turbulence conditions -- we must also include the vapor depletion

effect. By reducing the average saturation ratio to values below unity, vapor depletion further enhances the evaporation rate and the drift of droplets to smaller size. Thus it appears likely that the Kelvin effect and vapor depletion both contribute to balance the diffusive growth to larger droplet size during cloud droplet evolution.

4. Drift and diffusion for a prescribed droplet distribution

Let $w(z) = (4\pi/3)z^{3/2}$ be the droplet volume and consider an exponential stationary droplet volume distribution

$$n(w) = \frac{N_D}{a}\exp(-w/a) \tag{6.8}$$

normalized to N_D where $a = \langle w \rangle = L/N_D$ is the average droplet volume [2]. Equations 3.3 and 6.8 are identical except that the former is in terms of z and the latter w. By analogy, Eq. 6.8 is the solution to a Langevin equation having constant coefficients for drift and diffusion along the volume coordinate:

$$dw = \sigma_w dX + \bar{v}_w dt\,. \tag{6.9}$$

Transformation to the z coordinate following the rules of Ito calculus (Appendix A) gives

$$\begin{aligned} dz &= \sigma_w \frac{dz}{dw} dX + \left(\bar{v}_w \frac{dz}{dw} + \frac{1}{2}\sigma_w{}^2 \frac{d^2 z}{dw^2} \right) dt \\ &= \frac{1}{2\pi}\sigma_w z^{-1/2} dX + \frac{1}{2\pi}\left(\bar{v}_w z^{-1/2} - \frac{1}{8\pi}\sigma_w{}^2 z^{-2} \right) dt\,, \end{aligned} \tag{6.10}$$

exhibiting z-dependence in both the diffusion and drift coefficients. We do not attempt to offer a microphysical model in support of the complicated drift and diffusion coefficients appearing in Eq. 6.10, or even in the much simpler volume coordinate representation of Eq. 6.9: First, these coefficients are not unique as only their ratio is needed to specify the

distribution. Second, prescribed distributions are often based on fits to measurements and are thus themselves generally lacking a well understood microphysical foundation.

Construction of the corresponding Fokker-Planck equation (Eq. A.2 of Appendix A) is carried out using the new coefficients in Eq. 6.10 for $A(z)$ and $B(z)$, with Eqs. A.3 and A.4 used to obtain $D^{(2)}(z)$, and $D^{(1)}(z)$, respectively. The calculations are straightforward and yield the stationary solution in z:

$$f(z) = 2\pi \frac{N_D{}^2}{L} z^{1/2} \exp\left(-\frac{4\pi}{3L} N_D z^{3/2} \right), \tag{6.11}$$

which on variable transformation using $n(w) = f(z)dz/dw$ gives Eq. 6.8. In terms of the radial coordinate, Eqs. 6.8 and 6.11 take the form:

$$n_\infty(r) = 4\pi \frac{N_D{}^2}{L} r^2 \exp\left(-\frac{4\pi}{3L} N_D r^3 \right) \tag{6.12}$$

which is also a Weibull distribution, but with different exponents than Eq. 4.8 and narrower relative dispersion, $\varepsilon_\infty = 0.363...$.

Figure 5 presents a comparison of the three distributions from Eqs. 3.7, 6.4 and 6.12. The first two were derived on a microphysical basis whereas the third distribution was prescribed. All three distributions are in fact reasonable representations of typically encountered cloud droplet size distributions [10] and have relative spectral dispersions (summarized in the caption) in agreement with the range of observed values [6].

5. Summary and discussion

A new stochastic model has been introduced in this paper to represent the effects from fluctuations in water vapor saturation, due to turbulence, and depletion on the size

distribution of droplets in a cloud. Fluctuations in droplet size are modeled as Brownian diffusion, along the coordinate $z = r^2$, with a diffusion constant, D_Z, dependent on growth rate, variance of the fluctuations in saturation, and the fluctuation correlation time. An important property of turbulent condensation is that it provides a mechanism for droplets, even droplets initially of the same size, to grow at different rates as each droplet experiences, via Eq. 5.1, a different realization of the random distribution and a different growth/evaporation path and integrated droplet size. Diffusion of droplet size along the positive z coordinate would ordinarily lead to ever increasing total droplet volume were it not for the competing reduction in droplet size from the Kelvin and/or vapor depletion effects. The net result, confirmed here both by analytic calculations and Monte Carlo simulation is an evolution towards stationary droplet size distributions having properties (average size, relative dispersion, etc.) in good agreement with the observed properties of clouds.

The present stochastic theory for cloud droplet evolution also provides foundation for the recent kinetic potential (KP) theory of drizzle formation [1,2] as described in Appendix B. In that study, D_z was introduced as an empirical model parameter, and allowed to vary over a reasonable range of values, without further justification. The results of the present study represent a considerable advance in that D_Z has now been given a quantitative microphysical basis in terms of the condensation growth rate, and variance and correlation time of the fluctuations in supersaturation arising from turbulence. The analysis behind Fig. 4 shows explicitly the microphysical conditions under which the diffusive growth assumption used in McGraw and Liu [1,2] remains valid, while pointing the way to a more complete treatment (c.f. Sec. 2.2) should conditions be found for which the fluctuations in supersaturation decay over time scales comparable to or longer than those required for significant droplet growth.

The assumptions of fixed temperature, cloud droplet number, and liquid water content in the cloud parcel were made for convenience in introducing the new stochastic model, but are in no way essential to it. Future studies will apply the present parcel model to a rising and cooling parcel of cloud air and can also include the mixing effects from entrained air. The simplifying assumption of fixed droplet number avoids having to consider the activation of (or evaporation to) dry particles as well as the scavenging of

droplets through precipitation. The latter requires expanding the present cloud model to include the dynamics of precipitation and is a subject for future research.

Acknowledgements

The authors thank Drs. Peter H. Daum and Stephen E. Schwartz of BNL for encouragement and valuable discussions. This research was supported by the Office of Biological and Environmental Research of the US Department of Energy, as part of the Atmospheric Radiation Measurements (ARM) Program under contract DE-AC02-98CH10886.

References

1. R. McGraw, and Y. Liu, Analytic formulation and parameterization of the kinetic potential theory for drizzle formation, *Phys. Rev. E 70*, 031606 (2004).

2. R. McGraw, and Y. Liu, Kinetic potential and barrier crossing: a model for warm cloud drizzle formation, *Phys. Rev. Letts. 90*, 018501-1 thru 018501-4 (2003).

3. Climate Change 2001: The Scientific Basis. Contributions of Working Group I to the Third Assessment Report of the Intergovernmental Panel on Climate Change; Houghton, J. T., Ding, Y., Griggs, D. J., Noguer, M., van der Linden, P., Dai, X., Maskell, K., Eds. (Cambridge University Press, Cambridge, 2001).

4. R. A. Shaw, Particle-turbulence interactions in atmospheric clouds, *Annu. Rev. Fluid Mech. 35*, 183-227 (2003).

5. L. D. Rotstayn, and Y. Liu, A smaller global estimate of the second indirect aerosol effect. Geophys. Res. Lett., in press (2005). [BNL-73312-2004-JA-R1]

6. Y. Liu, and P. H. Daum, Spectral dispersion of cloud droplet size distributions and the parameterization of cloud droplet effective radius, *Geophys. Res. Letts. 27*, 1903-1906 (2000).

7. Y. Liu, and P. H. Daum, Parameterization of the autoconversion process. Part I: Analytical formulation of the Kessler-type parameterizations, *J. Atmos. Sci. 61*, 1539-1548 (2004).

8. Y. Liu, and P. H. Daum, Indirect warming effect from dispersion forcing, *Nature 419*, 580-581 (2002).

9. A. A. Costa, C. de Oliveira, J. de Oliveira, and A. Sampaio, Microphysical observations of warm cumulus clouds in Ceara, Brazil, *Atmos. Res. 54*, 167-199 (2000).

10. Y. Liu, L. You, W. Yang, and F. Liu, On the size distribution of cloud droplets, *Atmos. Res. 35*, 201-216 (1995).

11. Y. Liu and J. Hallett, The "1/3" power-law between effective radius and liquid water content, *Q. J. R. Meteor. Soc. 123*, 1789-1795 (1997).

12. W. E. Howell, The growth of cloud droplets in undiluted cloudy air, *J. Meteorol. Soc. 6*, 134-139 (1949).

13. X. Zhou, *Precipitation Formation of Warm Clouds*, (Scientific Publishing, 1964).

14. Y. S. Sedunov, *Physics of Drop Formation in the Atmosphere*, (Wiley, 1974).

15. W. A. Cooper, Effects of variable droplet growth histories on droplet size distributions. Part I: Theory, *J. Atmos. Sci. 46*, 1301-1311 (1989).

16. R. C. Srivastava, Growth of cloud drops by condensation: A criticism of currently accepted theory and a new approach, *J. of the Atmos. Sci. 46*, 869-887 (1989).

17. R. A. Shaw, W. C. Reade, L. R. Collins, and J. Verlinde, Preferential concentration of cloud droplets by turbulence: Effects on the early evolution of cumulus droplet spectra, *J. Atmos. Sci. 55*, 1965-1976 (1998).

18. M. B. Baker, R. G. Corbin, and J. Latham, The influence of entrainment on the evolution of cloud droplet spectra. I: A model of inhomogeneous mixing, *Quart. J. Roy. Meteor. Soc. 106*, 581-598 (1980).

19. E. Hicks, C. Pontikis, and A. Rigaud, Entrainment and mixing processes as related to droplet growth in warm midlatitude and tropical clouds, *J. Atmos. Sci. 47*, 1589-1618 (1990).

20. J. W. Telford, and S. K. Chai, A new aspect of condensation theory, *Pure Appl. Geophys. 118*, 720-742 (1980).

21. C. Su, S. K. Krueger, P. A. McMurtry, and P. H. Austin, Linear eddy modeling of droplet spectral evolution during entrainment and mixing in culumus clouds, *Atmos. Res. 47-48*, 41-58 (1998).

22. H. R. Pruppacher, and J. D. Klett, *Microphysics of Clouds and Precipitation* (Kluwer Academic, 1997).

23. V. I. Khvorostyanov, and J.A. Curry, Theory of Stochastic Condensation in Clouds. Part I: A General Kinetic Equation. *J. Atmos. Sci, 56*, 3985-3996 (1999).

24. V. I. Khvorostyanov, and J.A. Curry, Theory of Stochastic Condensation in Clouds. Part II: Analytical Solutions of the Gamma-Distribution Type. *J. Atmos. Sci, 56*, 3997-4013 (1999).

25. M. Kulmala, U. Rannik, E. L. Zapadinsky, and C. F. Clement, The effect of saturation fluctuations on droplet growth, *J. Aerosol Sci. 28*, 1395-1409 (1997).

26. T. K. Lesniewski, and S. K. Friedlander, Particle nucleation and growth in a free turbulent jet, *Proc. R. Soc. Lond. A454*, 2477-2504 (1998).

27. D. Chandler, *Introduction to Modern Statistical Mechanics* (Oxford University Press, New York, 1987) Pg. 251.

28. B. J. Berne and R. Pecora, *Dynamic Light Scattering* (Wiley, New York, 1976) Pg. 228.

29. R. Serra, M. Andretta, G. Zanarini, and M. Compiani, *Introduction to the Physics of Complex Systems*, (Pergamon, New York, 1986) chapt. 1.

30. P. Wilmott, S. Howison, and J. Dewynne *The Mathematics of Financial Derivatives* (Cambridge University Press, Cambridge, 1998) Chapt. 2.

31. H. Risken, *The Fokker-Planck Equation* (Springer-Verlag, New York, 1984).

32. R. McGraw, Description of aerosol dynamics by the quadrature method of moments, *Aerosol Sci. and Tech. 27*, 255-265 (1997).

33. D. H. Lenchow, J. Mann, and L. Kristensen, How long is long enough when measuring fluxes and other turbulence statistics*?, J. Atmos. Oceanic. Technol. 11*, 661-673 (1994).

34. D. T. Wu, Nucleation theory, *Solid State Phys. 50*, 37-187 (1997).

Appendix A: Ito calculus and the correspondence between Langevin and Fokker-Planck equations

Given a Langevin equation of the form

$$dz = A(z,t)dX + B(z,t)dt\ , \tag{A.1}$$

construction of the corresponding Fokker-Planck equation follows standard rules for handling stochastic differential equations (see, for example, Ref. 31 pgs 50 and 98):

$$\frac{\partial f}{\partial t} = \frac{\partial^2}{\partial z^2}\left(D^{(2)} f\right) - \frac{\partial}{\partial z}\left(D^{(1)} f\right) \tag{A.2}$$

with:

$$D^{(2)}(z) = \frac{A(z,t)^2}{2} \tag{A.3}$$

and, following the rules of Ito calculus,

$$D^{(1)}(z,t) = B(z,t)\ . \tag{A.4}$$

A factor of 1/2 appears in Eq. A.3 that does not appear in the definition of $D^{(2)}$ found in Ref. 31. This is due to the different normalization use here for the random increment dX (Eq. 2.15).

Comparing Langevin equations A.1 and 2.13, we obtain for this constant-coefficient case:

$$\begin{aligned} A(z) &= \sigma_Z \\ B(z) &= \bar{v} \end{aligned}$$

or

$$\begin{aligned} D^{(2)} &= \frac{A^2(z)}{2} = \frac{\sigma_Z^2}{2} = D_Z \\ D^{(1)} &= B(z) = \bar{v} \end{aligned}\ . \tag{A.5}$$

Substituting into the general form (Eq. A.2) immediately gives Eq. 3.1.

Given an original Langevin equation of the form A.1, and transformation function $w = w(z)$, the transformed Langevin equation is (Wilmott et al., 1995):

$$dw = A\frac{dw}{dz}dX + \left(B\frac{dw}{dz} + \frac{1}{2}A^2\frac{d^2w}{dz^2} \right)dt \qquad \text{(A.6)}$$

The second term in parenthesis is an additional contribution to drift motion that arises in the Ito calculus from Taylor expansion due to the fact that the expansion term of order dX^2 is retained (unlike in conventional calculus) because it is of order *dt*.

Appendix B: Relation to parameters used in the kinetic potential (KP) theory of drizzle formation

The kinetic potential, developed as a theoretical tool in nucleation theory [34], was recently used in the development of a new theory of drizzle formation [1,2]. In the KP drizzle theory, the size coordinate is descretized to a lattice and D_Z is determined from the hopping rate and jump distance between adjacent lattice sites. For example, with the lattice spacing $z_1 = r_1^2$ where r_1 is molecular radius of water, and nondimensional coordinate $h = z/z_1$, we obtain

$$D_Z = \beta^{cond} z_1^2 \tag{B.1}$$

where β^{cond} is the turbulent condensation transfer rate between adjacent lattice sites $h \to h+1$ [2]. The lattice is a mathematical construct whereas the diffusion coefficient is a physical quantity that, like all physical quantities encountered in the model, must be invariant to the choice of lattice spacing. Thus, for a z-independent D_Z, Eq. B.1 implies a z-independent transfer rate inversely proportional to the lattice spacing squared.

In addition to β^{cond} there are two additional transfer rates introduced to complete the KP drizzle model. These are the effective evaporation rate, γ^{eff}, giving the rate of back transfer ($h \leftarrow h+1$), and an additional contribution to the forward transfer rate ($h \to h+1$) from collection, β^{coll}. Collection refers to the gain in size of a specified drop large enough to have a significant gravitational fall velocity so as to accrete the smaller, slower falling, droplets that typify the main population of the cloud. Because drizzle formation is beyond the scope of the present study, we consider here only the two transfer rates, β^{cond} and γ^{eff}, which have the greatest influence on the droplet spectrum for non-precipitating clouds.

The principal advantage of the KP, $\Phi(z)$, is that it enables one to define a Boltzmann-type proportionality for the stationary cloud droplet population:

$$\frac{f_\infty(h+1)}{f_\infty(h)} = \exp\{-[\Phi(h+1)-\Phi(h)] = \frac{\beta^{cond}(h)}{\gamma^{eff}(h+1)}. \qquad \text{(B.2)}$$

In this way $\Phi(z)$ resembles a reduced thermodynamic potential but with broader utility as it is also defined (c.f. the second equality of Eq. B.2) solely in terms of transfer rates. The first and third terms satisfy the detailed balance condition:

$$\beta^{cond}(h) f_\infty(h) = \gamma^{eff}(h+1) f_\infty(h+1). \qquad \text{(B.3)}$$

A key result of the new stochastic model is that it provides a means to directly determine the effective evaporation rate. In our previous formulations [1,2], γ^{eff} was determined via the detailed balance condition and this, as seen from Eq. B. 3, requires *both* an estimate for the turbulent condensation transfer rate, β^{cond}, and specification of the cloud droplet size distribution. The new stochastic model also requires a determination for β^{cond} (equivalently, D_Z), but the cloud droplet size distribution is now a *derived* quantity determined by the model itself. Furthermore, D_Z has been given a more through microphysical basis in terms of the amplitude and persistence time of the turbulence fluctuations in *S* (Eq. 2.9). Finally, the new stochastic model provides foundation for the KP drizzle theory by showing explicitly how the barrier to drizzle formation [occurrence of a maximum in $\Phi(z)$] arises from the competition between water droplets for available vapor in the cloud. Specifically, the rising portion of the barrier is a consequence of vapor depletion as reflected in the negative drift velocity $\bar{v}_\infty$ in the stochastic model. This can be seen by substituting the derived expression for $f_\infty(z) = f_\infty(z_1 h) \equiv f_\infty(h)$ from Eq. 3.3 into Eq. B.2 to obtain:

$$\ln\left[\frac{f_\infty(h+1)}{f_\infty(h)}\right] = \frac{\bar{v}_\infty}{D_Z} z_1 = -[\Phi(h+1) - \Phi(h)] = -\frac{d\Phi}{dh} = -z_1 \frac{d\Phi}{dz} \qquad \text{(B.4)}$$

The second and fifth terms are readily integrated to obtain

$$\Phi(z) = \frac{|\bar{v}_\infty|}{D_Z} z \qquad \text{(B.5)}$$

where the constant of integration has been chosen such that the potential vanishes for $z = 0$. These results also yield the important inequality, $\beta^{cond}(h) < \gamma^{eff}(h+1)$, in the pre-collection regime due to the fact that $\bar{v}_\infty$ is negative, and $f_\infty(z)$ is in this model a decreasing function of z.

Equation B.5 gives a linear increase in potential with drop size that is the rising portion of the barrier to drizzle formation in the full KP drizzle theory (McGraw and Liu, 2004). Thus it is the physics of drift and diffusion behind Eq. B. 5 that both determines the Boltzmann exponential factor, shaping the cloud droplet distribution (cf. Eq. 3.5), and is responsible for the activation barrier to drizzle formation. The main difference between Eq. B.5 and the full KP is that the latter also includes collection. Nevertheless, Eq. B.5 remains an excellent approximation to the full KP over the range of typical cloud droplet sizes and collection is not important in this regime. Collection results in a downturn in the full KP, corresponding to activationless growth, in the size regime of the larger falling drops that are beyond the scope of the present study (McGraw and Liu, 2004).

Figure captions:

Figure 1. Temperature dependent diffusion-controlled growth prefactor used in Eq. 2.1. Solid curve includes properties of water and the coupling of heat and mass transfer fluxes that arise during growth/evaporation of the drop. Results for P = 800mb.

Figure 2. (Top) Stationary cloud droplet size distribution from Eq. 3.3 for a mean droplet radius of 10 micron and normalization to unity. Arrows show balance of currents from diffusion and drift. (Bottom) Same as above except plotted versus the radial coordinate $r = +\sqrt{z}$. The distribution in terms of the radial coordinate takes the Weibull form.

Figure 3. (Top) Cumulative radial distribution versus scaled drop radius from Eq. 4.7 (solid curve) and comparison with results from four 100-drop Monte-Carlo simulations (points) at different times near $\tilde{t} = 4$. (Bottom) Relative dispersion, ε, for 100-drop samples taken at reduced time increments of 0.001 (5000 samples total) as a function of reduced sample time. Results are shown for evolution from an initially monodisperse size distribution.

Figure 4. Contours of constant $t_{1\%}$, solid curves, and τ, dashed curves, as a functions of the logarithm (base 10) $\sigma_S^{\,2} / \gamma$ (in seconds) and temperature (in degrees C). See text for definition of $t_{1\%}$ and Table 1 for definition of τ.

Figure 5. Comparison of normalized droplet radius distributions. The reduced radius is defined as $\tilde{r} = r / \bar{r}$ where $\bar{r}$ is the mean radius for the distribution. Solid curve, depletion distribution from Eq. 3.7; dashed curve, Kelvin effect distribution from Eq. 6.4; dotted curve, exponential volume distribution from Eq. 6.12. Relative dispersions are 0.52, 0.71, and 0.36, respectively.

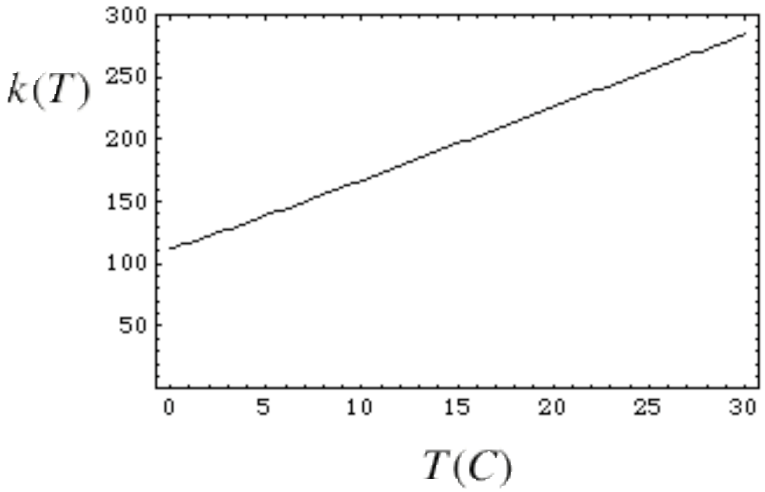

Figure 1

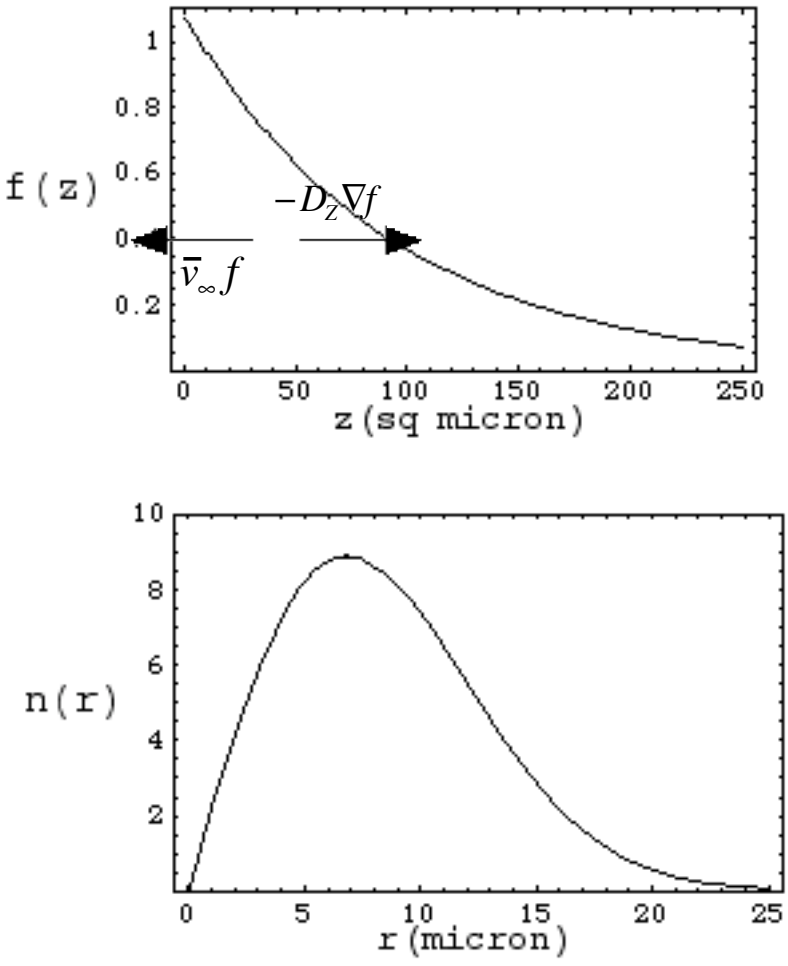

Figure 2

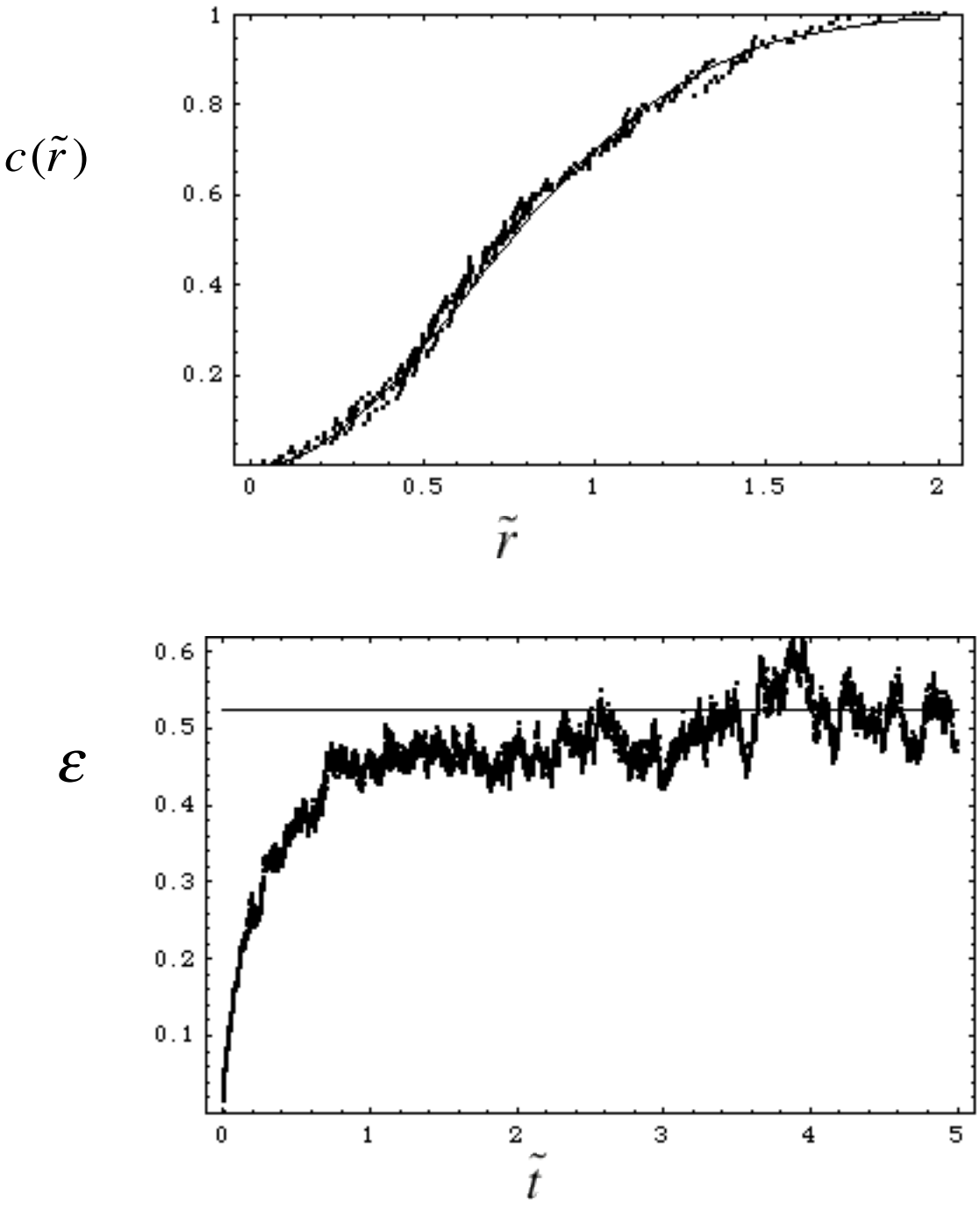
$c(\tilde{r})$
1
0.8
0.6
0.4
0.2
0
0.5
1
1.5
2
$\tilde{r}$
ε
0.6
0.5
0.4
0.3
0.2
0.1
0
1
2
3
4
5
$\tilde{t}$

Figure 3

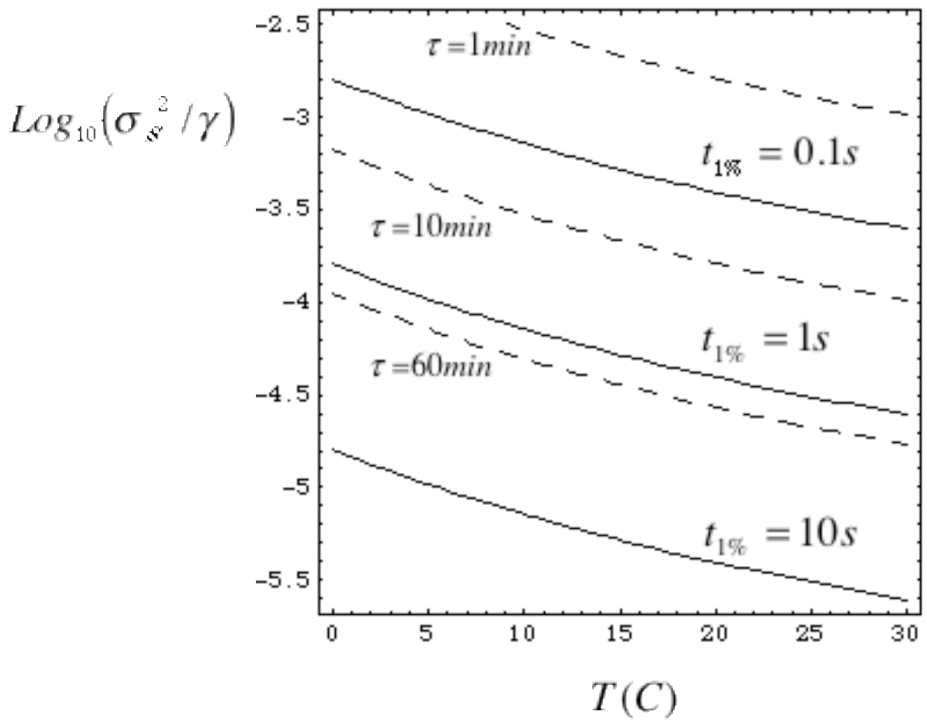

Figure 4

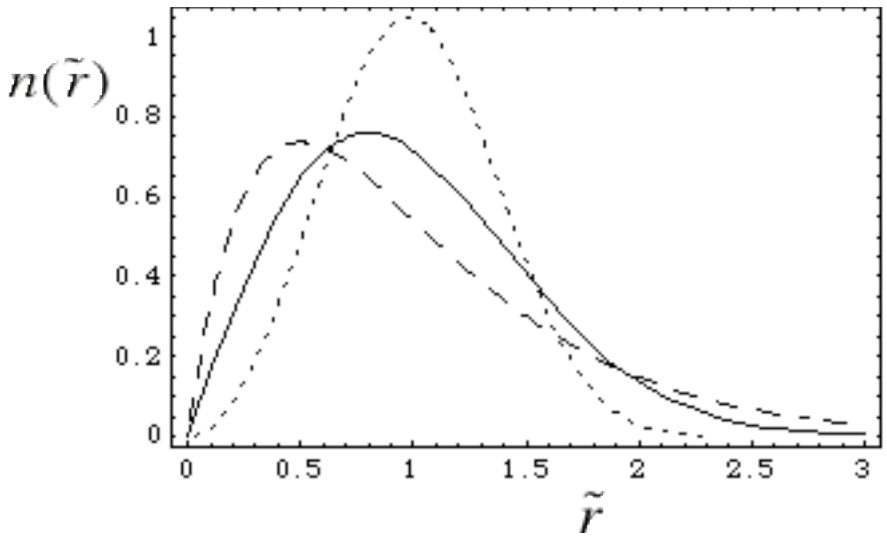

Figure 5